# Lecture 4:
# organic semiconductor/metal interfaces
# Chapter 2 & Chapter 3

Ref.
1. M. Knupfer and H. Peisert, phys. stat. sol. (a) 201, 1055 (2004).
2. H. Ishii, N. Hayashi, E. Ito, Y. Washizu, K. Sugi, Y. Kimura, M. Niwano, Y. Ouchi, and K. Seki, phys. stat. sol. (a) 201, 1075 (2004)
3. H. Ishii, K. Sugiyama, E. Ito, and K. Seki, Adv. Mater. 11, 605 (1999).

**2009. 3. 12 & 3.17.**

Changhee Lee
School of Electrical Engineering and Computer Science
Seoul National Univ.
chlee7@snu.ac.kr



## Simple band diagrams typically used for the organic devices



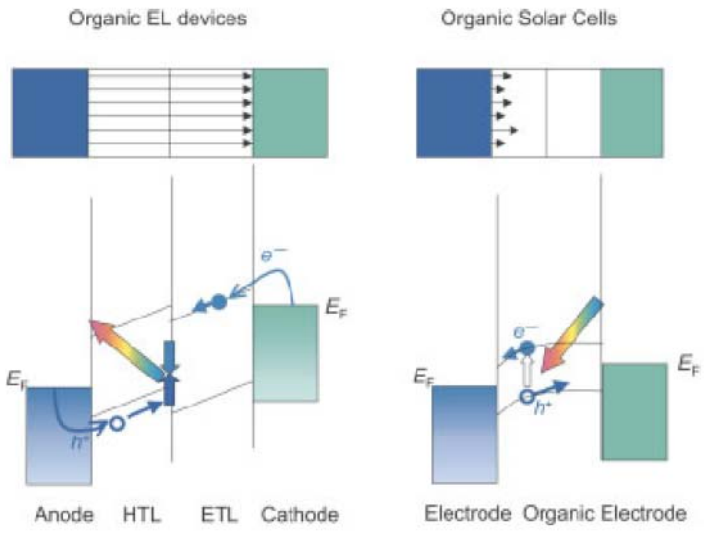


. H. Ishii, N. Hayashi, E. Ito, Y. Washizu, K. Sugi, Y. Kimura, M. Niwano, Y. Ouchi, and K. Seki, phys. stat. sol. (a) 201, 1075 (2004)

# Energy band structures with metal contacts



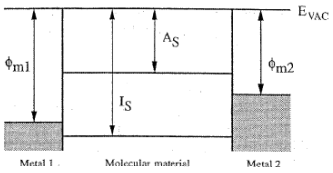


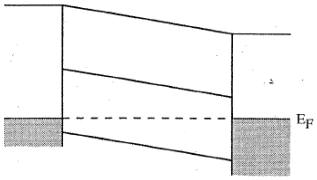


**Flat band** Internal Field = $(\phi_{m1}-\phi_{m2})/d$

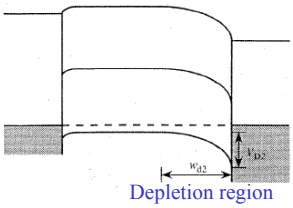


Depletion region

**Schottky barrier**

Fermi level is equalized throughout the M/S/M structure by the diffusion of the carriers: Diffusion of holes from the molecular material into the metals leaves the negative ionized acceptor dopants at the interface **(band bending)**: This diffusion will continue until the internal energy barrier ($eV_D$: diffusion potential) is large enough to stop it.

$$\phi_B^{+} = I_S - \phi_m = qV_D + E_F^{P} \qquad w_d = [\frac{2\varepsilon_o\varepsilon_r(V_D - kT/q)}{qN_a}]^{1/2}$$



# Charge density



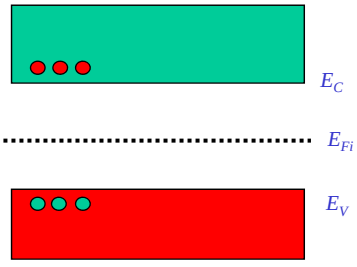


Intrinsic Semi.

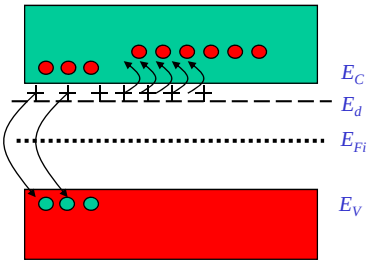


extrinsic Semi.

$$n_0 p_0 = n_i^2$$

$$n_0 = \frac{N_d - N_a}{2} + \sqrt{\left(\frac{N_d - N_a}{2}\right)^2 + n_i^2}$$

$$p_0 = \frac{N_a - N_d}{2} + \sqrt{\left(\frac{N_a - N_d}{2}\right)^2 + n_i^2}$$

# Built-in potential and width of space charge region

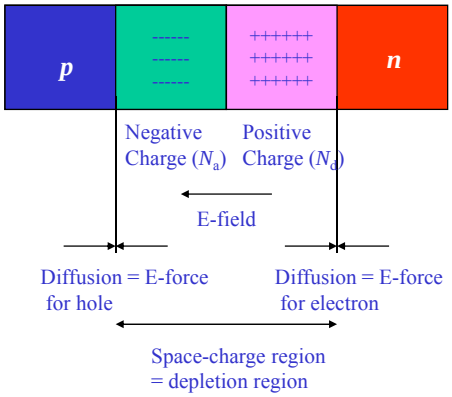


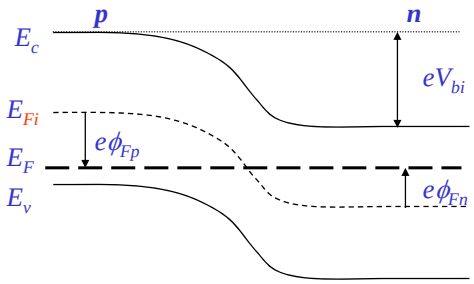


$$V_{bi} = |\phi(x = x_n)| = \frac{e}{2\varepsilon_s}(N_d x_n^2 + N_a x_p^2)$$

$$W = \left\{ \frac{2\varepsilon_s V_{bi}}{e} \frac{N_d + N_a}{N_d N_a} \right\}^{1/2}$$



# Measurement of an acceptor density at interfaces



Al/PPV/ITO Schottky diode

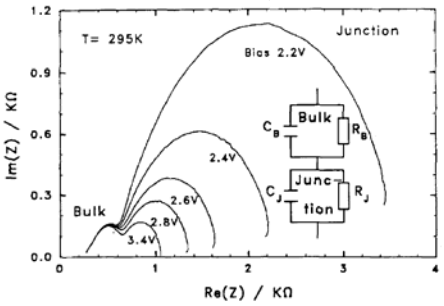


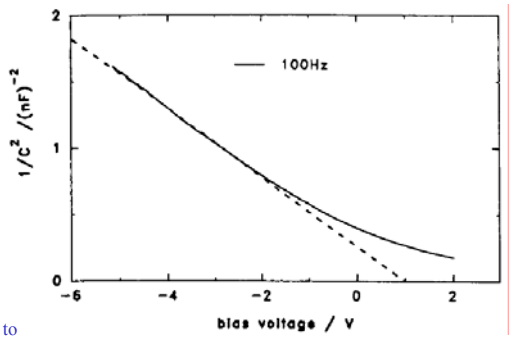


Under reverse bias the measured capacitance corresponds to the junction capacitance, which can be expressed according to the Schottky model

$$\frac{C}{A} = \left(\frac{e\varepsilon_o\varepsilon_r N_a}{2} \times \frac{1}{V_d + V}\right)^{1/2}$$

$$w = \left[\frac{2\varepsilon_o\varepsilon_r (V_d + V)}{eN_a}\right]^{1/2}$$

$N_a \approx 10^{17}\, cm^{-3}$,

Built-in voltage or diffusion voltage $V_d \approx 1$ V,

$w = 0.1\,\mu m$

S. Karg, W. Riess, V. Dyakonov, M. Schwoerer, *Synth. Met.*, **54**, 427 (1993).

# Fermi level alignment at the metal/semiconductor contact

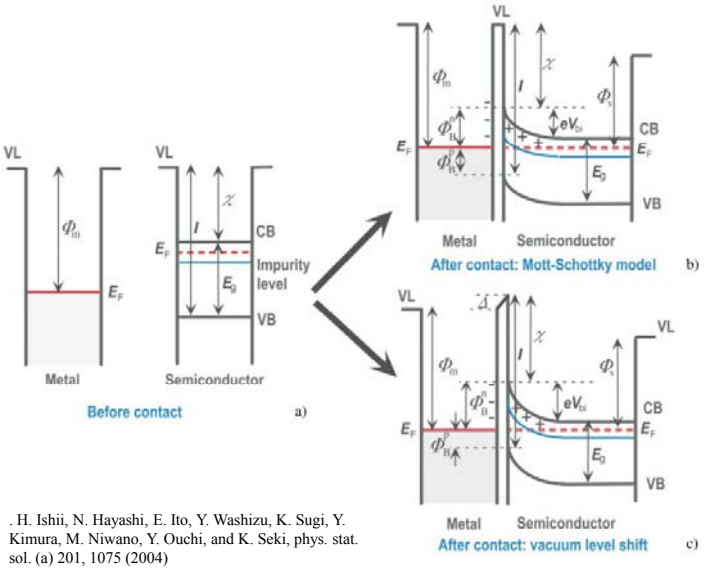


. H. Ishii, N. Hayashi, E. Ito, Y. Washizu, K. Sugi, Y. Kimura, M. Niwano, Y. Ouchi, and K. Seki, phys. stat. sol. (a) 201, 1075 (2004)

$\phi_m$: 금속의 work function
$\phi_s$ : 반도체의 work function
$\chi$:electron affinity

Barrier height for e injection
$\Phi_{Bn} = \Phi_m - \chi$

built-in potential
$eV_{bi} = |\Phi_m - \Phi_s|$

Formation of interface dipole inducing vacuum level shift ($\Delta$)
→Barrier height is modified:
$\Phi_{Bn} = \Phi_m + \Delta - \chi$
→$V_{bi}$ is also modified:
$eV_{bi} = |\Phi_m + \Delta - \Phi_s|$





# XAS and PES

• XAS (X-ray absorption spectroscopy): measure the absorption of the x-rays (from synchrotron radiation light source) due to electron excitations from occupied into unoccupied levels as a function of the energy.
• Element-specific information about the electronic structure.
• Due to the selection rules the orientation of molecular adsorbates can be investigated.
→ polarization dependent XAS: an important tool for the investigation of the geometry of molecular adsorbates, especially for ultra-thin coverages.

• PES (Photoemission spectroscopy): Determination of band offsets at semiconductor heterojunctions and at metal/semiconductor interfaces

Schematic representation of XAS

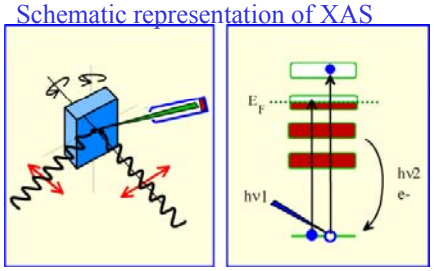


Schematic representation of PES

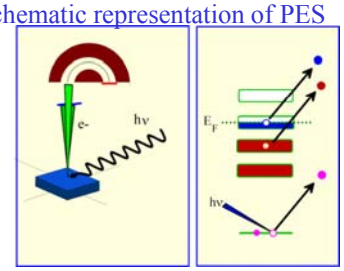

# Polarization dependent XAS



Possible core excitations into vacant states are governed by selection rules, such as the change of the quantum number of the angular momentum ($\Delta l = \pm 1$) or the direction of the electric vector ***E*** of the linearly polarized synchrotron radiation.

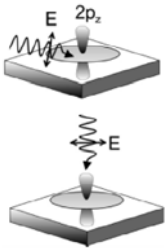


the chosen angle of incidence favors either excitations into the π* (top) or the σ* (bottom) orbitals.

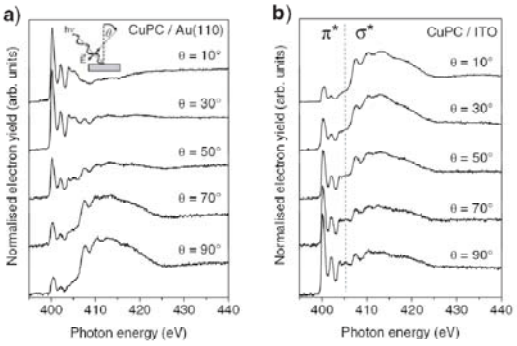


**Fig. 4** Series of N1s excitation spectra of CuPc films grown on (a) Au(110) and (b) ITO as a function of the angle $\theta$ between the surface normal and the electric field vector of the soft X-ray radiation [57]. The lower energy features (398–405 eV) represent the $\pi^*$ resonances, whereas those features above 405 eV are related to the $\sigma^*$ resonances.

The organic molecules are well ordered on *both* substrates, but the adsorbate geometry in each case is radically different: for Au(110) the CuPc molecular plane is parallel to the substrate surface and for ITO it is perpendicular.

M. Knupfer and H. Peisert, phys. stat. sol. (a) 201, 1055 (2004).



# The molecular orientation of CuPc



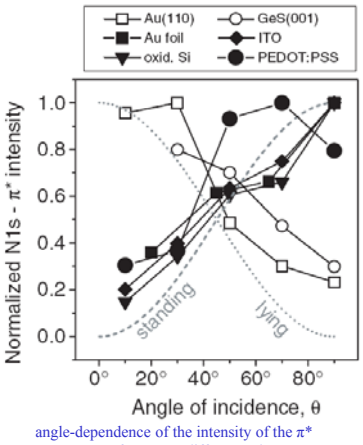


angle-dependence of the intensity of the π* resonances of CuPc on different substrates.

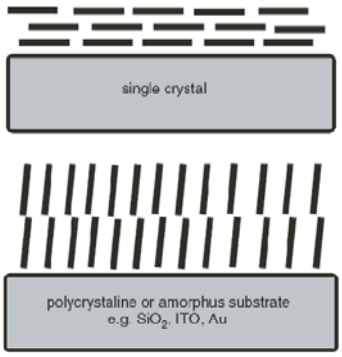


**Fig. 7** Schematic representation of the adsorption geometry of CuPc molecules on technical substrates (standing) and on single crystalline substrates (lying).

• If the molecule-substrate interaction is stronger than the molecule-molecule interaction, the adsorption of the molecule occurs in a lying geometry (i.e. the molecular plane is parallel to the substrate surface).
• If the molecule-substrate interaction is weak, as in the case of van-der-Waals substrates, then increased tilt-angles of 10–25 ° have been observed. For thicker films of NiPc on HOPG, even a standing molecular orientation has been proposed.

M. Knupfer and H. Peisert, phys. stat. sol. (a) 201, 1055 (2004).

## PES

• The measured kinetic energy ($E_{kin}$) allows the determination of the binding energy ($E_B$) of the photoelectron via a simple equation:

$$E_B = h\nu - E_{kin} - \varphi_{SP}$$

where hν is the photon energy and $\varphi_{SP}$ is a spectrometer specific constant, the work function of the spectrometer.

• The very small escape depth of the photoelectrons is responsible for the surface sensitivity of the method.

• $E_B(i) = E(N-1, i) - E(N) = -\varepsilon(i) + R_D$, where $-\varepsilon(i)$ is the orbital energy and $R_D$ an additional relaxation contribution

M. Knupfer and H. Peisert, phys. stat. sol. (a) 201, 1055 (2004).





## Workfunction & IP Measurement: Photoelectric effect

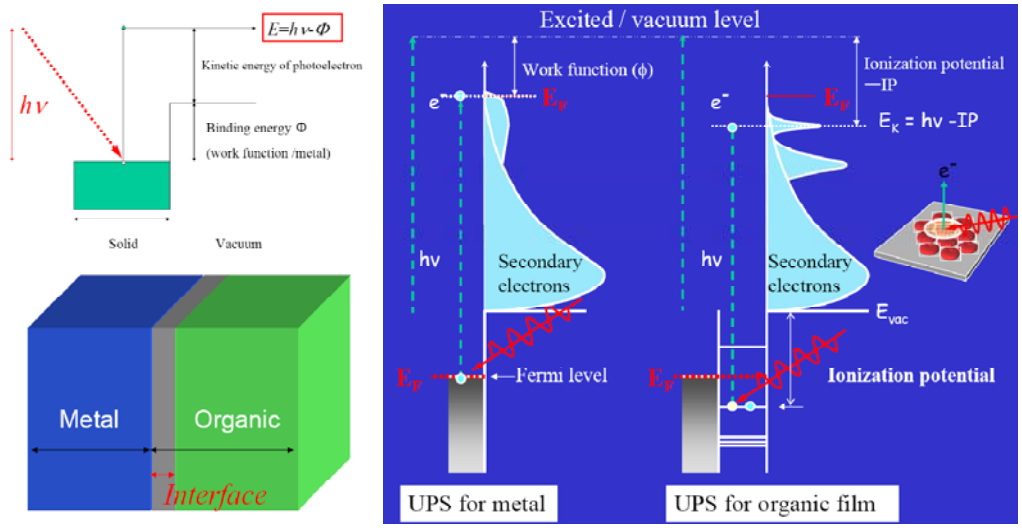


*Energy level alignment at interface: Molecular orientation, reaction with metal, distortion of electronic distribution, existence of electric dipoles, etc.*

## Kelvin Probe Method

"The Kelvin Probe is a non-contact, non-destructive measurement device used to investigate properties of materials. It is based on a vibrating capacitor and measures the work function difference, or for non-metals, the surface potential, between a conducting specimen and a vibrating tip. The work function is an extremely sensitive indicator of surface condition and is affected by adsorbed or evaporated layers, surface reconstruction, surface charging, oxide layer imperfections, surface and bulk contamination, etc. The Kelvin method was first postulated by the renowned scottish scientist Lord Kelvin, in 1898."

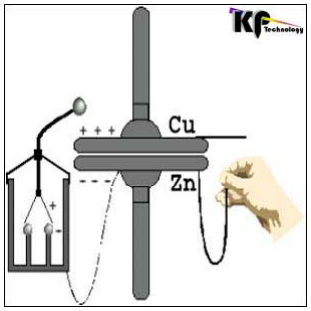


*The original apparatus of Lord Kelvin (1898).*

http://www.kelvinprobe.info/

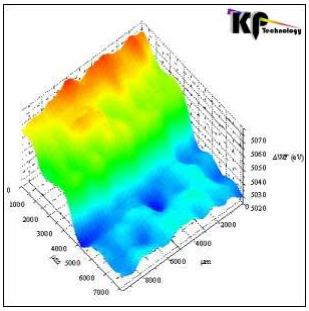

*100nm ITO on glass - Sample courtesy of Dr. Dmitry Poplavskyy, **OSRAM** Opto Semiconductors Inc.*

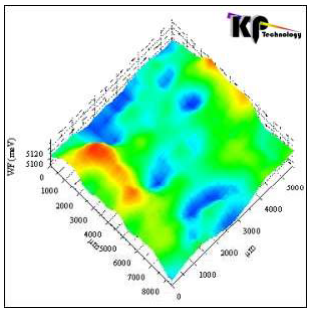

*100nm PEDOT:PSS - Sample courtesy of Dr. Dmitry Poplavskyy, **OSRAM** Opto Semiconductors Inc.*





## Principle of Kelvin probe measurements

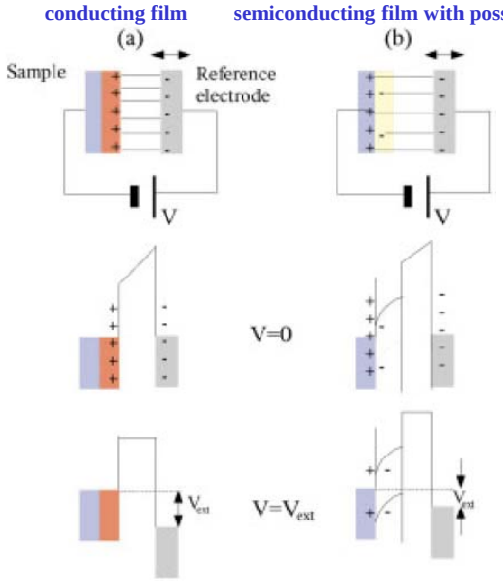


**The contact potential is formed under zero bias voltage.**

**Under an adjusted bias voltage, the electric field in the gap becomes null. When null signal is detected in KP measurements, the alignment of the vacuum level of the sample film and the reference electrode is guaranteed.**

# Measurement of an internal electric field

## Electroabsorption Measurement

a.c. Field $E = E_{dc} + E_{ac}\cos(\Omega t)$

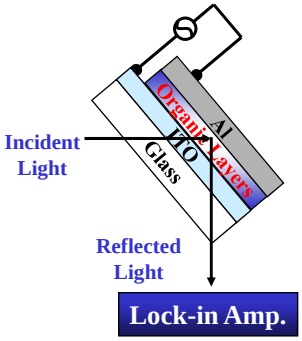


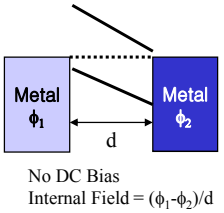


No DC Bias
Internal Field = $(\phi_1-\phi_2)/d$

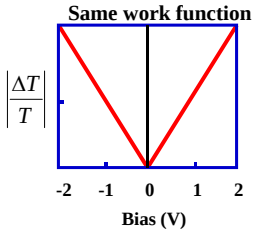


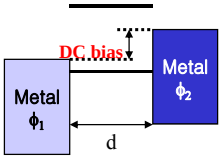


DC bias = $(\phi_1-\phi_2)/d$
Internal Field = 0

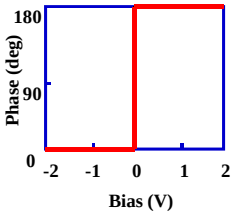


Electroabsorption response to an E field

$$\Delta\alpha(h\nu) \propto -\frac{\Delta T}{T}(h\nu) \propto \mathrm{Im}\,\chi^{(3)}(h\nu)E^2$$





# Measurement of an internal electric field

Al/MEH-PPV/Al

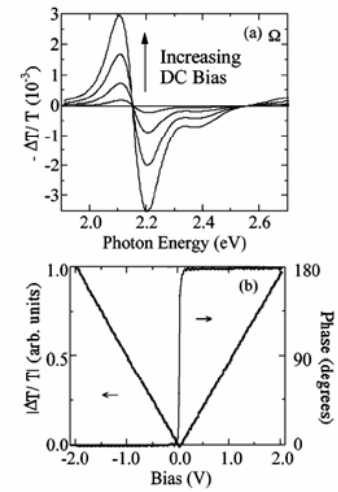


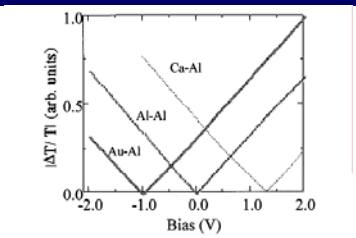


**FIGURE 5.** Magnitude of the electroabsorption response at 2.1 eV as a function of bias for three metal/MEH–PPV/Al structures.

**TABLE 1.** Work Function Difference, $\Delta\phi$, and Electroabsorption Zero Field Bias, $V_0$, for a Series of Metal Contact Pairs to MEH–PPV

| Contact metals | $\Delta\phi$ | $V_0$ |
|---|---|---|
| Au–Al | −0.8 | −1.0 |
| Al–Al | 0.0 | 0.0 |
| Ca–Al | 1.4 | 1.3 |
| Sm–Al | 1.6 | 1.3 |
| Ag–Ca | 1.4 | 1.4 |
| Cu–Ca | 1.7 | 1.7 |
| Au–Ca | 2.2 | 2.0 |
| Pt–Ca | 2.7 | 2.1 |

Ian H. Campbell, John P. Ferraris, Thomas W. Hagler, Michael D. Joswick, Ian D. Parker, Darryl L. Smith
Polymers for Advanced Technologies, **8** (7), pp. 417 – 423

# Internal electric field and accumulated charges

**MULTILAYER ORGANIC LED**

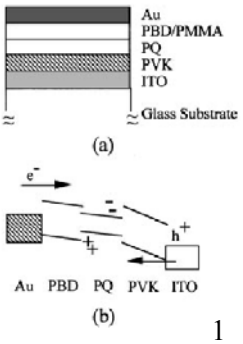


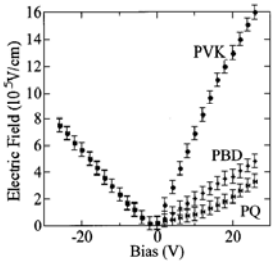


**FIGURE 9.** Electric field as a function of d.c. bias voltage in each layer of the LED. The a.c. bias amplitude was 3 V.

$$\sigma = \frac{1}{4\pi}\Delta(\varepsilon E_{dc})$$

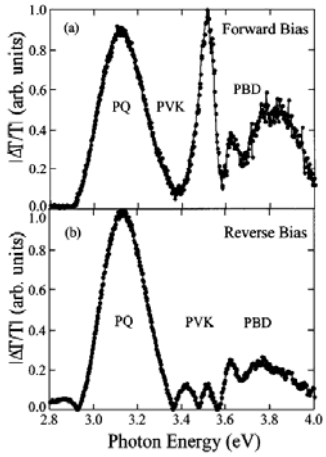


**FIGURE 8.** Electroabsorption spectra of the three layer LED under (a) 20 V forward bias and (b) −20 V reverse bias at the fundamental frequency of the applied a.c. bias. The relative changes in the amplitudes of the signal from each layer are evident. The a.c. bias amplitude was 3 V.

At the largest forward bias voltage measured,
electron density at the PQ/PVK interface: $2\times10^{12}$ electrons/cm$^2$

hole density at the PBD/PQ interface: $3\times10^{11}$ holes/cm$^2$.

I.H. Campbell, M.D. Joswick, I.D. Parker, Appl. Phys. Lett. 67 (1995) 3171.





# Average internal electric field in organic layers of OLED

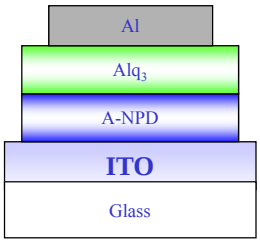


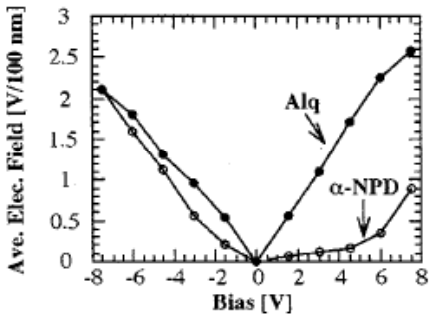


FIG. 8. Average electric field in the $\alpha$-NPD layer (open circles) and in the Alq layer (closed circles) of an $\alpha$-NPD/Alq double-layer device as a function of dc bias.

In double-layer a-NPD/Alq devices,
the average E field in the a-NPD layer is considerably smaller compared to that in the Alq layer in forward bias,
whereas the average electric field in the Alq layer is identical to that in the a-NPD layer in reverse bias.

F. Rohlfing, T. Yamada, T. Tsutsui, J. Appl. Phys. 86 (1999) 4978.

## Photovoltaic measurement of the built-in potential



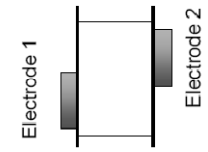


Open circuit conditions

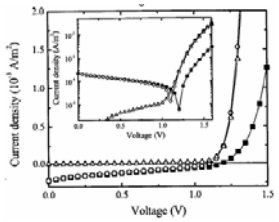


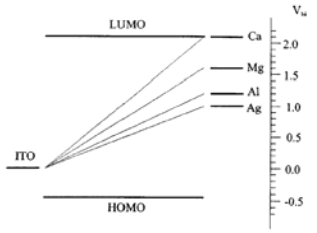


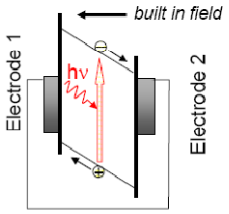


Short circuit conditions

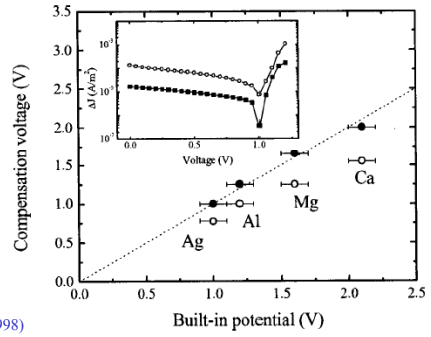


G. G. Malliaras, J. R. Salem, P. J. Brock, and J. C. Scott, J. Appl. Phys. **84**, 1583 (1998)



## Energy levels of Organic Materials



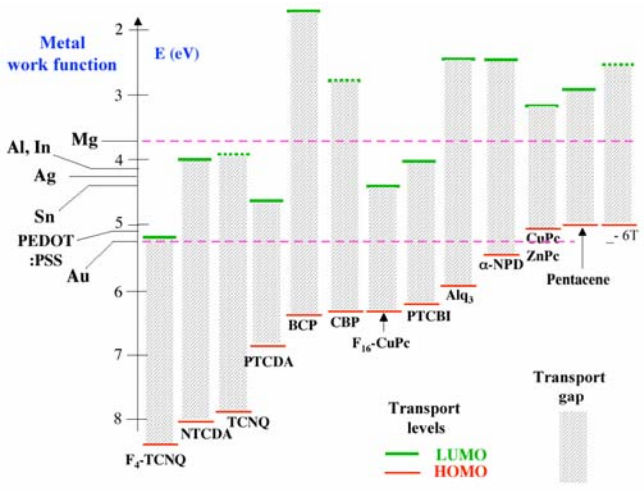


*Weiying Gao and Antoine Kahn (Princeton Univ.)*, NSF workshop, "Technological Challenges for Flexible, Light-weight, Low-cost and Scalable Organic Electronics and Photonics," January 16-17, 2003

Ionization Potential (eV)

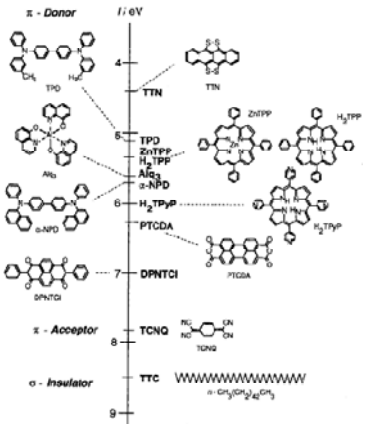


H. Ishii, K. Sugiyama, E. Ito, and K. Seki, Adv. Mater. **11**, 605 (1999).

## Does band bending occur in organic semiconductors?



• HOMO-LUMO gap of organic semiconductors is large (2–3 eV).

The concentration of thermally excited carriers is extremely small like an insulator.

→ Band bending effect is usually neglected at insulator/organic interfaces.

• Fermi level alignment requires thermal equilibrium:

In organic semiconductors, molecules are bound only by van der Waals force so that wave function and charge density are fairly localized within each molecule.

→ Carrier exchange process between adjacent molecules is not effective in contrast to the case of inorganic semiconductors with good conductivity.

→ Thus it is not apparent that unbalance in Fermi level can be compensated by the redistribution of carriers.



## Energy level alignment at interfaces (TPD on Au) using PES



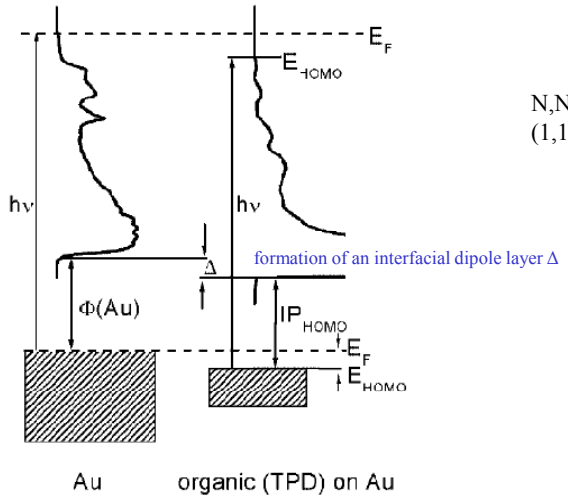


N,N'-diphenyl-N,N'-bis (3-methylphenyl)–(1,1') –biphenyl-4,4'diamine

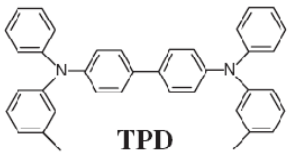


**TPD**

M. Knupfer and H. Peisert, phys. stat. sol. (a) 201, 1055 (2004).

# Effect of interface dipole



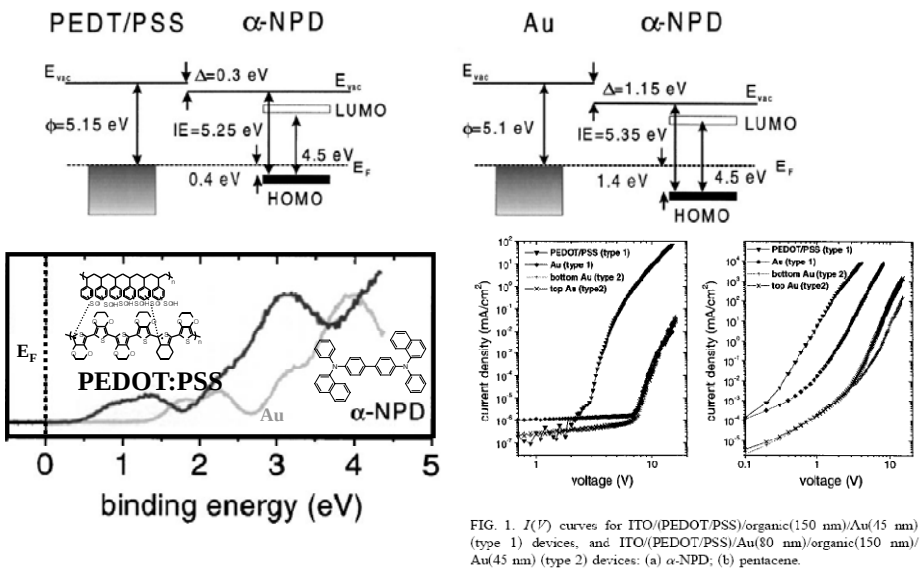


FIG. 1. $I(V)$ curves for ITO/(PEDOT/PSS)/organic(150 nm)/Au(15 nm) (type 1) devices, and ITO/(PEDOT/PSS)/Au(80 nm)/organic(150 nm)/Au(45 nm) (type 2) devices: (a) α-NPD; (b) pentacene.

N. Koch, A. Kahn, J. Ghijsen and J.-J. Pireaux, J. Schwartz, R. L. Johnson, A. Elschner, Appl. Phys. Lett. **82**, 70 (2003)



# Metal/Organic interface



**Schottky-Mott model**
Common vacuum level assumption

**Interface Dipole Model**

$$\Delta = N\frac{p}{\varepsilon_i}$$

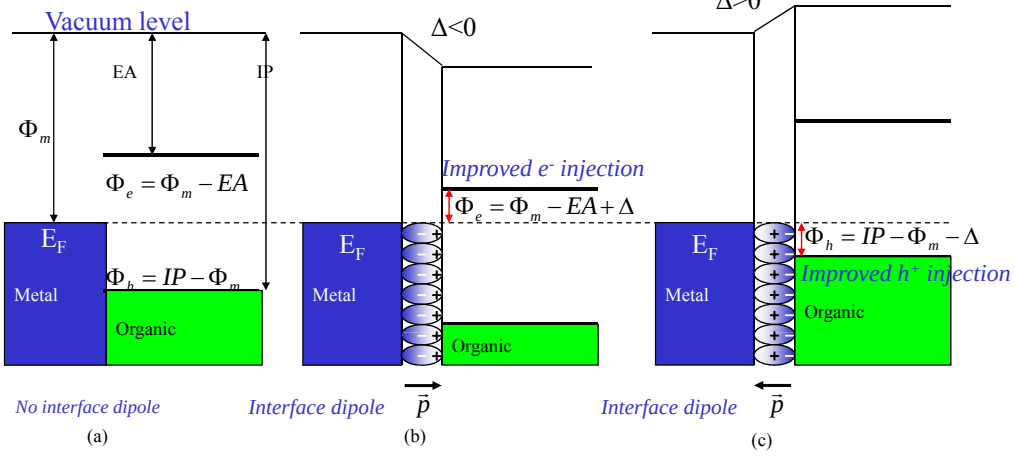


I. H. Campbell, S. Rubin, T. A. Zawodzinski, J. D. Kress, R. L. Martin, D. L. Smith, N. N. Barashkov, and J. P. Ferraris, Phys. Rev. B 54, R14321 (1996).

# Potential barrier at metal/Alq3 interfaces



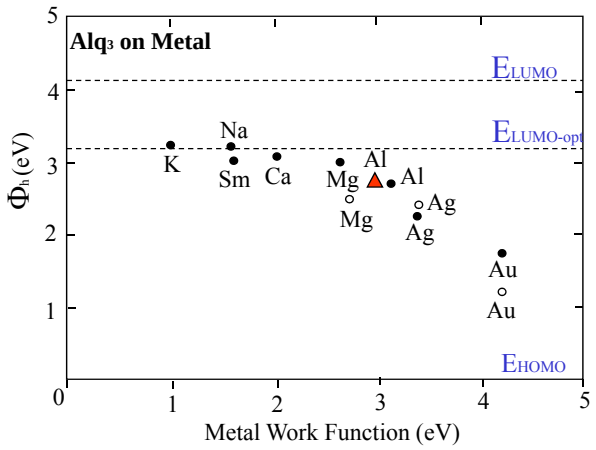


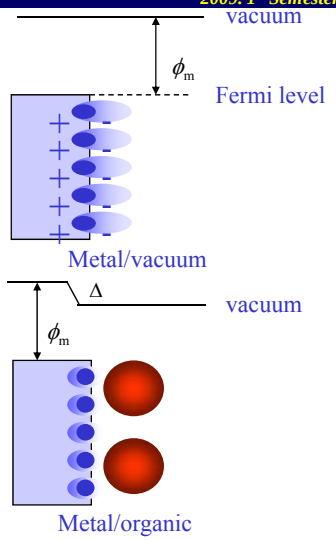


Tang, Lee, et al. Chem. Phys. Lett, 396, 92 (2004)
Hill et al. Appl. Phys. Lett. 73, 662 (1998)
Isjii et al. Adv. Mater. 11, 605 (1999)

Part of the tailing of electrons at the material surface is compressed back into the metal.
→ Interface dipole Δ is formed.



# Origin of interface dipole



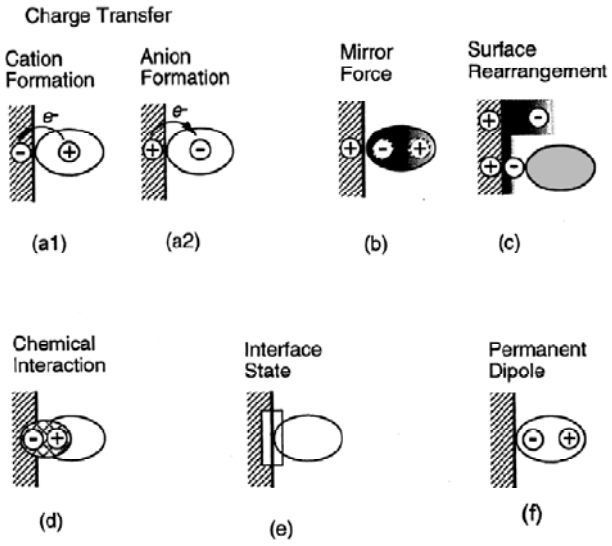


Possible factors forming and affecting the interfacial dipole layer.
a1) and a2): Charge transfer across the interface,
b) Concentration of electrons in the adsorbate leading to positive charging of the vacuum side,
c) Rearrangement of electron cloud at the metal surface, with the reduction of tailing into vacuum,
d) Strong chemical interaction between the surface and the adsorbate leading to the rearrangement of the electronic cloud and also the molecular and surface geometries (both directions of dipoles possible),
e) Existence of interface state serving as a buffer of charge carriers,
f) Orientation of polar molecules or functional groups.

H. Ishii, K. Sugiyama, E. Ito, and K. Seki, Adv. Mater. **11**, 605 (1999).

# Examples: CuPC/Au interfaces

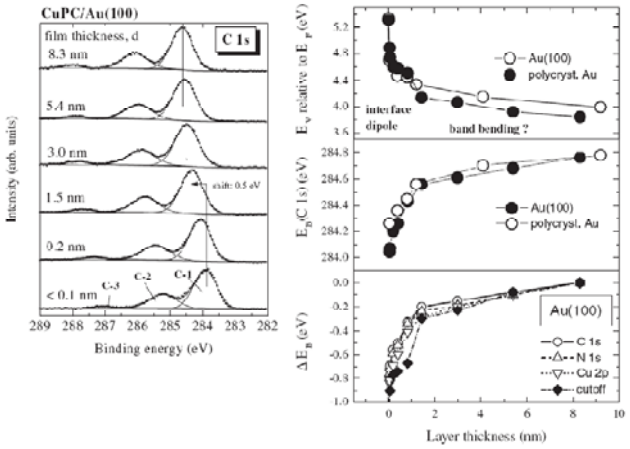


**Fig. 9** C 1s XPS spectra ($h\nu = 1486.6$ eV) of CuPc on Au(100) [70]. The spectra for low coverages are strongly shifted to lower binding energies. The absence of additional features at the earliest stages of deposition and the only very small broadening rule out chemical interactions at the interface.

**Fig. 10** Comparison of the energy level shifts of CuPc on gold as obtained from XPS and UPS measurements [70].

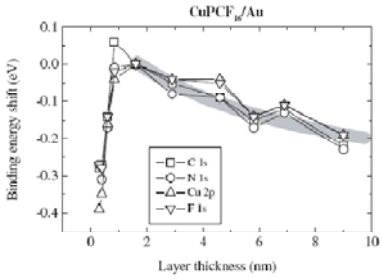


M. Knupfer and H. Peisert, phys. stat. sol. (a) 201, 1055 (2004).





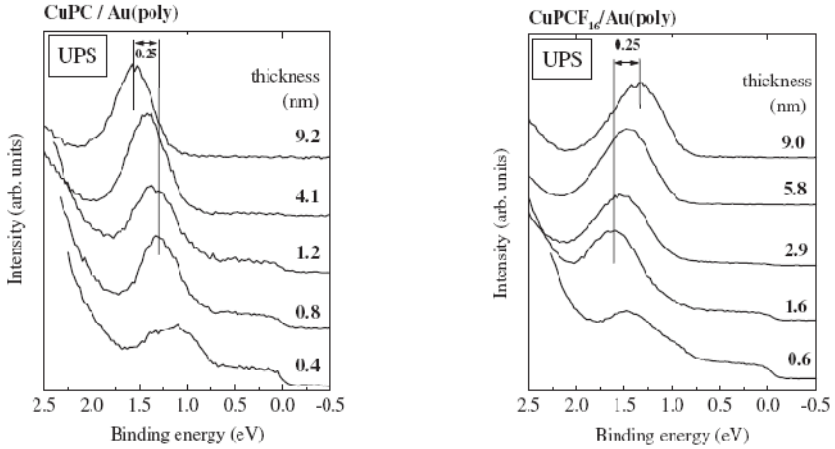


**Fig. 12** Valence band photoemission spectra of CuPc (left panel) and $CuPcF_{16}$ (right panel) deposited on gold as a function of film thickness.

M. Knupfer and H. Peisert, phys. stat. sol. (a) 201, 1055 (2004).

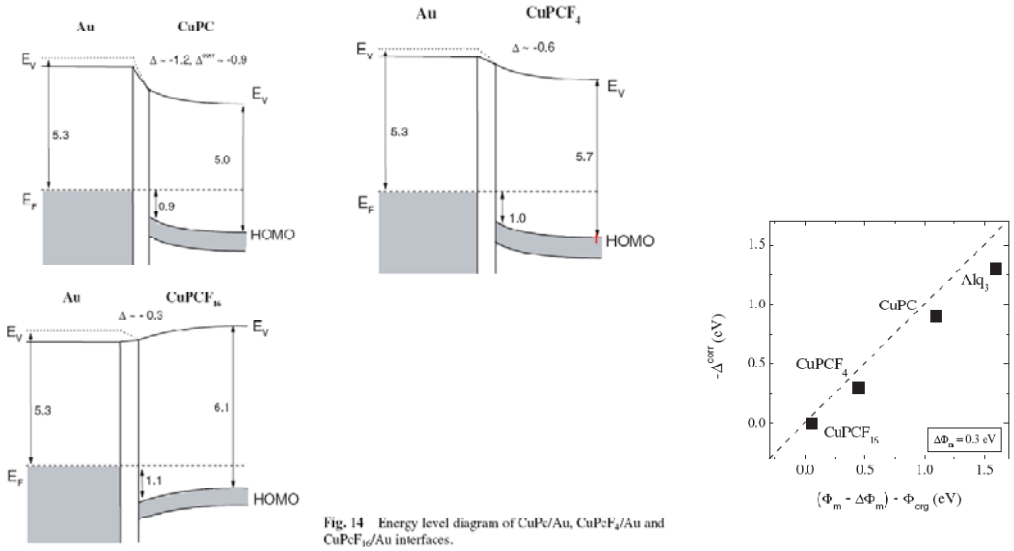


Fig. 14 Energy level diagram of CuPc/Au, $CuPcF_4$/Au and $CuPcF_{16}$/Au interfaces.

M. Knupfer and H. Peisert, phys. stat. sol. (a) 201, 1055 (2004).



## Reactive surfaces: indium-tin oxide



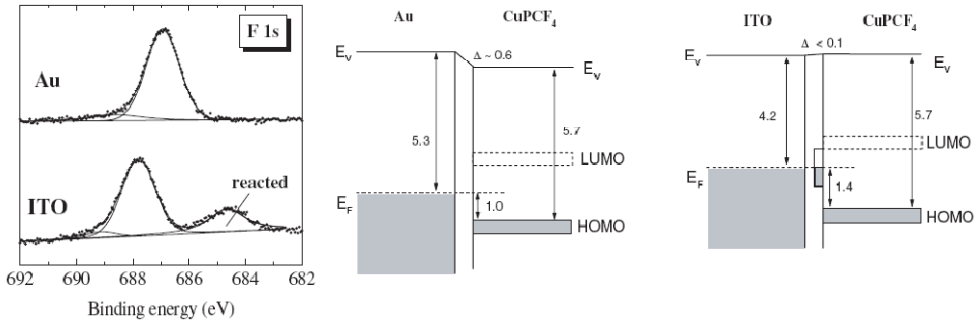


F 1s core level spectra for ultrathin CuPcF4 films (about 0.3–0.4 nm) on Au and on ITO.

M. Knupfer and H. Peisert, phys. stat. sol. (a) 201, 1055 (2004).

## Reactive surfaces: PEDOT:PSS

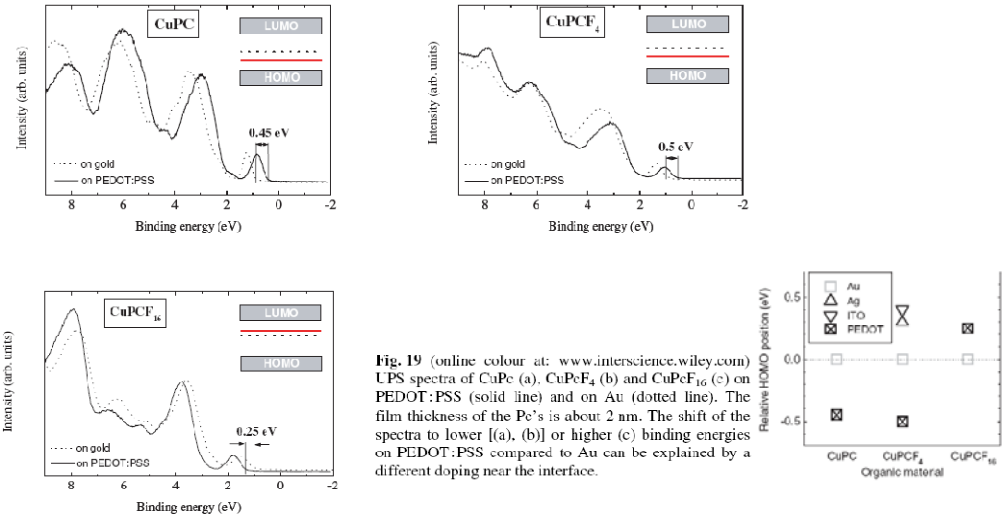


**Fig. 19** (online colour at: www.interscience.wiley.com) UPS spectra of CuPc (a), $CuPcF_4$ (b) and $CuPcF_{16}$ (c) on PEDOT:PSS (solid line) and on Au (dotted line). The film thickness of the Pc's is about 2 nm. The shift of the spectra to lower [(a), (b)] or higher (c) binding energies on PEDOT:PSS compared to Au can be explained by a different doping near the interface.

M. Knupfer and H. Peisert, phys. stat. sol. (a) 201, 1055 (2004).





## C60/metal interface: case of band bending

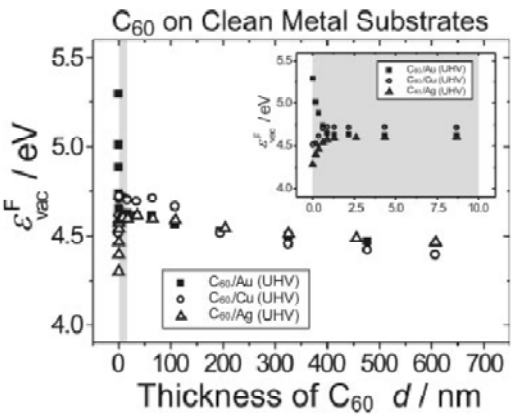


**Fig. 4** Variation in $\varepsilon^F_{vac}$ for $C_{60}$ on Au, Cu, and Ag as a function of the thickness of $C_{60}$, $d$. The data in the region for small $d$ up to 10 nm is shown in the inset.

. H. Ishii, N. Hayashi, E. Ito, Y. Washizu, K. Sugi, Y. Kimura, M. Niwano, Y. Ouchi, and K. Seki, phys. stat. sol. (a) 201, 1075 (2004)

## C60/metal interface



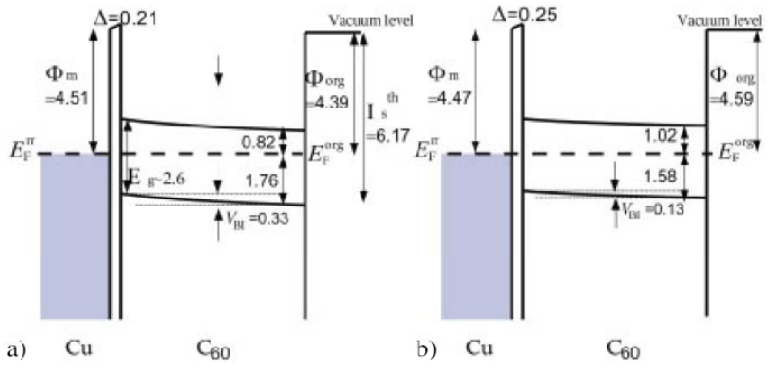


Energy diagrams of Cu/C60 interfaces obtained from the KP measurements in the case of
(a) as-received and
(b) Once-purified C60.

. H. Ishii, N. Hayashi, E. Ito, Y. Washizu, K. Sugi, Y. Kimura, M. Niwano, Y. Ouchi, and K. Seki, phys. stat. sol. (a) 201, 1075 (2004)



## TPD/metal interface



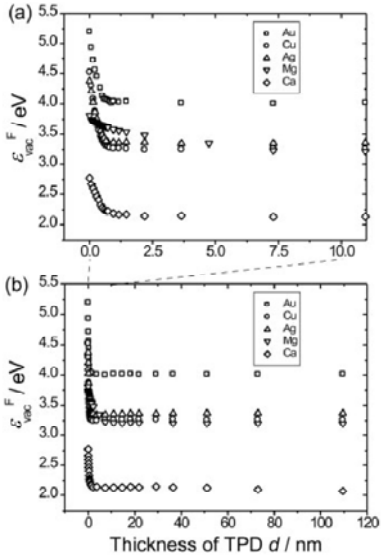


Variation in $E^F_{vac}$ for TPD on Au, Cu, Ag, Mg and Ca substrates as a function of TPD thickness, d.
(a) The region for small d up to 10 nm is expanded.
(b) The whole region upto d = 110 nm.

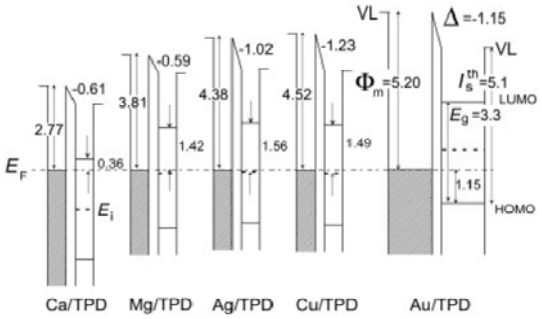


Energy diagram of TPD/metal (Au, Cu, Ag, Mg and Ca) interfaces constructed from the results of KP measurements.

. H. Ishii, N. Hayashi, E. Ito, Y. Washizu, K. Sugi, Y. Kimura, M. Niwano, Y. Ouchi, and K. Seki, phys. stat. sol. (a) 201, 1075 (2004)

## Potential gradient built in Alq3 film

Variation of $E^F_{vac}$ of Alq3 film deposited on Au and Al as a function of the film thickness. The deposition of Alq3 was performed in dark condition.

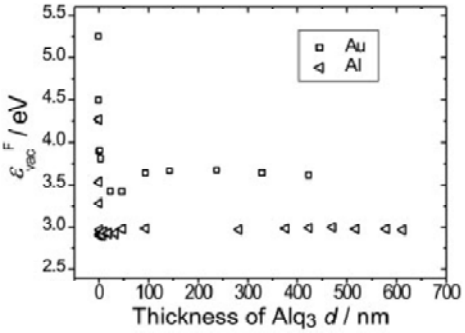


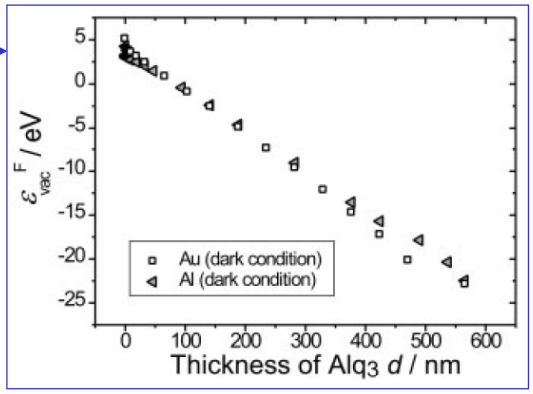


**Fig. 8** Variation of $\varepsilon^F_{vac}$ of $Alq_3$ film deposited on Au and Al as a function of the film thickness. The deposition of $Alq_3$ was performed under light irradiation.

. H. Ishii, N. Hayashi, E. Ito, Y. Washizu, K. Sugi, Y. Kimura, M. Niwano, Y. Ouchi, and K. Seki, phys. stat. sol. (a) 201, 1075 (2004)





## Potential gradient built in Alq3 film

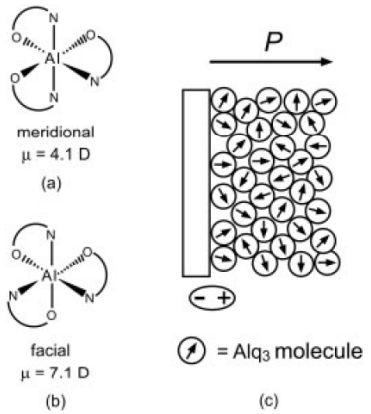


**Fig. 10** Two isomeric forms of $Alq_3$: (a) meridional and (b) facial. Model of the formation of giant surface potential of $Alq_3$ film is shown in (c).

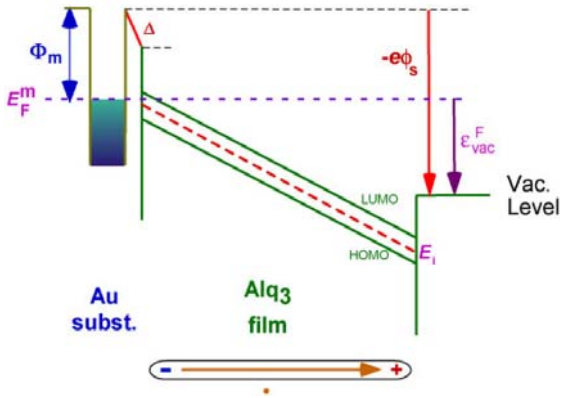


. H. Ishii, N. Hayashi, E. Ito, Y. Washizu, K. Sugi, Y. Kimura, M. Niwano, Y. Ouchi, and K. Seki, phys. stat. sol. (a) 201, 1075 (2004)

## Potential gradient built in Alq3 film

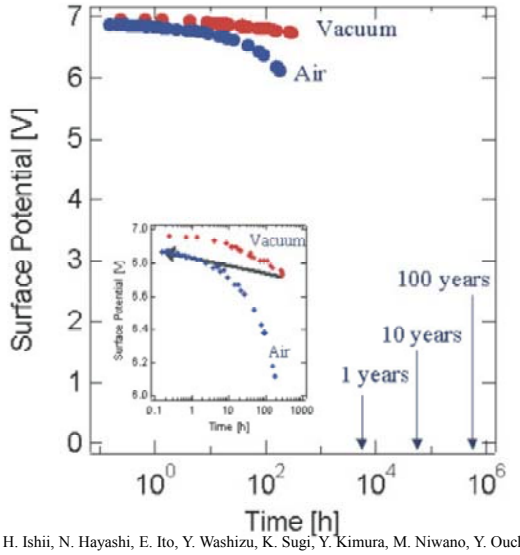


**Fig. 12** (online colour at: www.interscience.wiley.com) The change of the surface potential of $Alq_3$ film in vacuum after the deposition in dark condition [49]. After keeping vacuum condition for 200 hours, the chamber is purged and the sample was kept in atmosphere.

. H. Ishii, N. Hayashi, E. Ito, Y. Washizu, K. Sugi, Y. Kimura, M. Niwano, Y. Ouchi, and K. Seki, phys. stat. sol. (a) 201, 1075 (2004)



Organic Semiconductor
EE 4541.617A
2009. 1st Semester

## Potential gradient built in Alq3 film

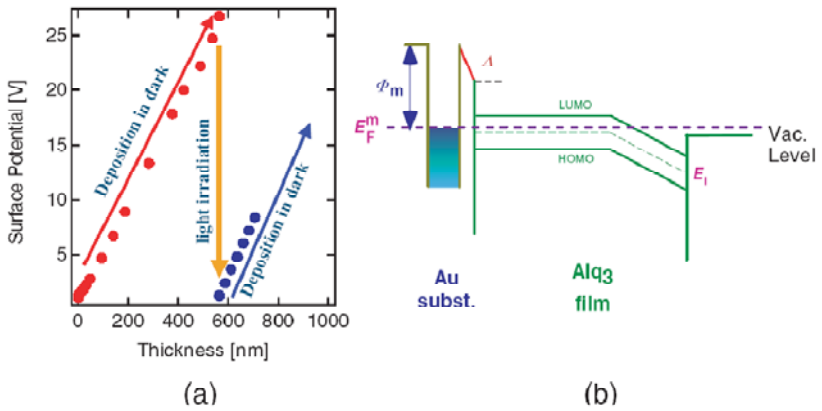


**Fig. 14** (online colour at: www.interscience.wiley.com) The change of the surface potential of $Alq_3$ film is plotted as a function of the film thickness (a) and the energy diagram constructed from the result (b). The large SP formed by deposition in dark was once removed by light irradiation. Additional deposition on the film induced the increase of the SP again.

. H. Ishii, N. Hayashi, E. Ito, Y. Washizu, K. Sugi, Y. Kimura, M. Niwano, Y. Ouchi, and K. Seki, phys. stat. sol. (a) 201, 1075 (2004)

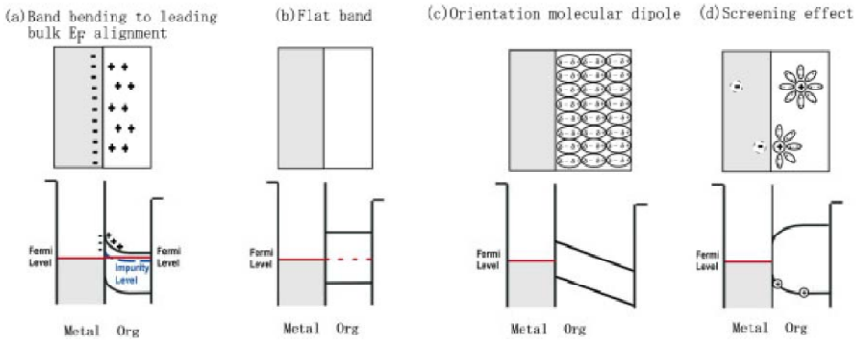


**Fig. 15** (online colour at: www.interscience.wiley.com) Various type of band bending at organic semiconductor/metal interfaces. (a) Impurity-derived band bending leading to the bulk Fermi level alignment. (b) Flat band case due to high purity of organic semiconductor. (c) Linear potential profile observed for $Alq_3$ film evaporated in dark condition. (d) Band bending effect in broad sense due to screening effect of carriers near metal electrode.

. H. Ishii, N. Hayashi, E. Ito, Y. Washizu, K. Sugi, Y. Kimura, M. Niwano, Y. Ouchi, and K. Seki, phys. stat. sol. (a) 201, 1075 (2004)